Self-Assembly of Periodic Serrated Nanostructures

Dongdong Li,[†,‡] Chuanhai Jiang,[‡] Jianhua Jiang,[‡] and Jia G. Lu*[,†]

Department of Physics & Astronomy, University of Southern California, Los Angeles, California 90089-0484, and School of Materials Science and Engineering, Shanghai Jiao Tong University, Shanghai 200240, China

Received August 15, 2008. Revised Manuscript Received September 26, 2008

Anodic aluminum oxide membranes with serrated nanochannels have been successfully fabricated via a two-step annodization method. The serrated channels with periodic intervals are aligned at an angle of ~25° along the stem channels. The formation of the serrated channels is attributed to the generation of oxygen gas bubbles and the resulted compressive stress on the oxide membrane. To reveal the inside channel structure, platinum is electrodeposited into the template. The as-synthesized serrated Pt nanowires demonstrate a superior electrocatalytic activity due to significantly enhanced electric field strength around serrated tips. Moreover, hierarchical serrated/straight hybrid structures are constructed using this simple and innovative self-assembly technique.

1. Introduction

Self-assembled nanoporous anodic aluminum oxide (AAO) membrane with straight channels has long been an important tool in synthesizing highly ordered and vertically aligned quasi-one-dimensional nanostructures for various applications.[1−6] Recently shape-selective nanomaterials have been achieved using AAO as a template.[7−12] It is envisioned that nanowires with multibranches will significantly increase the active functional sites for applications as sensors, catalysts, chemical cells, and so forth. The pore diameter and interpore distance can be controlled by the anodization voltage with respective proportionality constants of ~0.9 and 2.5 nm/V.[13] And it has been shown that reducing the anodic voltage by a factor of $1/\sqrt{n}$ leads to Y-branched ($n = 2$) and multibranched ($n > 2$) nanochannel arrays, as demonstrated in the synthesis of Y-shaped and hierarchically branched metal nanowires[7−11] and carbon nanotubes.[11,12] However, due to the nature of those fabrication processes, the branches are typically limited to form only at the boundary of the adjacent oxide layers which are anodized under different voltages.

Herein, we present a simple and cost-effective approach to fabricate AAO membranes with periodic serrated nanochannels. These innovative structures provide paradigms to study the formation process of AAO membranes and to design serrated nanowires with enhanced functionality. To illustrate the serrated nanostructures, metals, such as Pt, Cu, and Co, have been deposited into the serrated anodic alumina template by an electroplating method. In this report, we present serrated Pt nanowires which demonstrate an outstanding catalytic activity compared with straight Pt nanowires.

2. Experimental Section

2.1. Synthesis of AAO Membranes. Straight and serrated AAO templates are systematically synthesized via a two-step anodization method under a wide process window with the anodizing voltage from 10 to 80 V. In this experiment, aluminum foils (0.3 mm thickness, 99.999% purity) are first anodized in 0.3 M oxalic acid at 60 V and 5 °C. The as-formed porous layer is then etched by a mixture of 1.8 wt % H_2CrO_4 and 6.0 wt % H_3PO_4 at 60 °C. The second anodization step performed under the same condition leads to highly ordered straight channels,[6,14] whereas conducting the second step in 6.0 wt % aqueous phosphoric acid solution at 60 V and 22 °C yields serrated anodic alumina (SAA) membranes. The interpore distance (depicting pore density) and membrane thickness of the SAA are similar to those of the straight channeled AAO. Multilayer (i.e., straight + serrated) hybrid structures are productively created by applying the respective procedures sequentially.

2.2. Synthesis and Characterization of Pt Nanowire Arrays. A gold (Au) layer (200 nm) is evaporated onto the as-formed AAO template to serve as the working electrode. A copper wire is then bonded onto the Au electrode by conductive silver paint. The Au covered AAO is epoxy- bonded to a polyvinylchloride plastic substrate and submerged into $HgCl_2$ to remove the Al substrate.

* To whom correspondence should be addressed. E-mail: jia.grace.lu@usc.edu.
† University of Southern California.
‡ Shanghai Jiao Tong University.

(1) Taberna, P. L.; Mitra, S.; Poizot, P.; Simon, P.; Tarascon, J.-M. *Nat. Mater.* **2006**, *5*, 567.
(2) Umeda, R.; Awaji, H.; Nakahodo, T.; Fujihara, H. *J. Am. Chem. Soc.* **2008**, *130*, 3240.
(3) Salem, A. K.; Searson, P. C.; Leong, K. W. *Nat. Mater.* **2003**, *2*, 668.
(4) Lee, K. B.; Park, S.; Mirkin, C. A. *Angew. Chem., Int. Ed.* **2004**, *43*, 3048.
(5) Van Quy, N.; Hoa, N. D.; Yu, W. J.; Cho, Y. S.; Choi, G. S.; Kim, D. *Nanotechnology* **2006**, *17*, 2156.
(6) Liu, Z.; Chang, P.-C.; Chang, C.-C.; Galaktionov, E.; Bergmann, G.; Lu, J. G. *Adv. Funct. Mater.* **2008**, *18*, 1.
(7) Choi, J.; Sauer, G.; Nielsch, K.; Wehrspohn, R. B.; Gosele, U. *Chem. Mater.* **2003**, *15*, 776.
(8) Mahima, S.; Kannan, R.; Komath, I.; Aslam, M.; Pillai, V. K. *Chem. Mater.* **2008**, *20*, 601.
(9) Gao, T.; Meng, G.; Zhang, J.; Sun, S.; Zhang, L. *Appl. Phys. A: Mater. Sci. Process.* **2002**, *74*, 403.
(10) Tian, Y. T.; Meng, G. W.; Biswas, S. K.; Ajayan, P. M.; Sun, S. H.; Zhang, L. D. *Appl. Phys. Lett.* **2004**, *85*, 967.
(11) Meng, G. W.; Jung, Y. J.; Cao, A. Y.; Vajtai, R.; Ajayan, P. M. *Proc. Natl. Acad. Sci. U.S.A.* **2005**, *102*, 7074.
(12) Li, J.; Papadopoulos, C.; Xu, J. *Nature* **1999**, *402*, 253.
(13) Nielsch, K.; Choi, J.; Schwirn, K.; Wehrspohn, R. B.; Gösele, U. *Nano Lett.* **2002**, *2*, 677.
(14) Chang, P. C.; Chen, H. Y.; Ye, J. S.; Sheu, F. S.; Lu, J. G. *ChemPhysChem* **2007**, *8*, 57.

10.1021/cm8022242 CCC: $40.75
Published on Web 12/31/2008

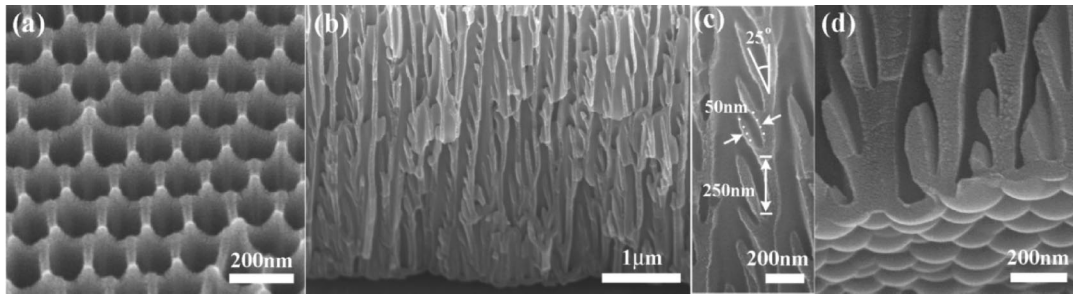

Figure 1. SEM images of (a) top view and (b) cross section view of free-standing SAA membrane. Close-up views of the (c) middle and (d) bottom section of the membrane in (b).

Afterward, the barrier layer is removed by an ion-milling process. Both straight and serrated Pt nanowires are fabricated by electrodeposition into the straight and serrated channels, respectively. The electrolyte used in the process consists of 5 mM H_2PtCl_6 and 0.1 M HCl in deionized water. In the experiment, alternating voltage (1 Hz) electrodeposition, with −350 mV offset and 50 mV amplitude at room temperature, is utilized to enhance ionic diffusion in the serrated channels.

The electrocatalytic activities of serrated and straight wires are characterized for methanol oxidation in a conventional three-electrode system, where the Pt nanowires are employed as the working electrode, Ag/AgCl saturated in 3 M NaCl as the reference electrode, and a platinum wire as the counter electrode. Cyclic voltammetry measurements of straight and serrated Pt nanowire arrays were carried out in N_2 saturated 2 M CH_3OH + 0.1 M H_2SO_4 solution at a scan rate of 50 mV/s and 22 °C. Corresponding chronoamperometric experiments of the Pt nanowire arrays were performed at 0.66 V with respect to the reference.

3. Results and Discussion

The scanning electron microscopy (SEM) images in Figure 1 show typical free-standing SAA templates. Figure 1a displays the hexagonal close packed lattice structure. Figure 1c is an enlarged image corresponding to the middle section of the SAA shown in Figure 1b. All the branches are inclined with an angle ranging from 20 to 30° to the stem-channel. The average channel spacing (D_c), width (W_c), and length (L_c) of the parallel stem-channels are around 150 nm, 80 nm, and 4 μm, respectively, while those of the branch-channels are about 250 nm, 50 nm, and 250 nm, respectively. The wall thickness of the stem-channels is about 50 nm which is consistent with that of the serrated channels. Figure 1d displays the SAA bottom view, indicating that the serrated structures initiate to form at the bottom of the membranes.

This unique structure establishes a new perspective to understand the formation mechanism of anodic aluminum oxide. It has been generally accepted that porous structures are formed when films are developed in acid solutions.[15−18] Nanochannels grow perpendicular to the aluminum substrate surface under the equilibrium of oxide growth at the metal/oxide interface and field-enhanced oxide dissolution at the oxide/electrolyte interface.[19,20] Recently a field-assisted flow model is presented using a tracer study.[21,22] The generation and development of pores are mainly ascribed to the plastic flow of alumina from the center of the pore bottom to the pore wall due to the accumulated compressive stress. However, these studies on the channel formation only address the evolution of straight walled channels and self-assembly ordering in two-dimensions and are not sufficient to explain the assembly of serrated structures along the nanochannels.

From our experiment, we conclude that the formation of serrated channels arises from the evolution of oxygen bubbles during the anodization in phosphoric acid. It is known that the oxygen bubbles are the origin of the void creation in barrier[23,24] and porous-type membranes.[25] In the anodization process, aluminum oxide is formed ($3O^{2-} + 2Al^{3+} \rightarrow Al_2O_3$) at the metal/oxide interface via the transfer of Al^{3+} and O^{2-} ions across the barrier layer, and O_2 is generated in the oxide as a byproduct ($2O^{2-} \rightarrow O_2 + 4e^-$).[23,26] Since the electric field strength is the strongest at the pore bottom,[20] O^{2-} ions are easily oxidized there to generate O_2 bubbles.

As illustrated in Figure 2, the initially formed bubbles with small sizes are trapped inside the barrier layer. The subsequent oxidization of O^{2-} contributes to the expansion of the as-formed oxygen bubbles, instead of generating new bubbles due to the relatively high nucleation energy. When the bubble sizes reach the barrier thickness (∼50 nm), oxygen gas will release from the barrier layer and create a mold for serrated channels. Taking into account the surface energy of the alumina, the gas pressure in an O_2 bubble of ∼50 nm in diameter is estimated to be ∼160 MPa.[23,24] The compressive stress accumulated from the evolution of gas bubbles deforms the gel-like alumina.[27,28] In the experiment, the Al foils are placed vertically in the electrochemical cell (as illustrated

(15) Masuda, H.; Satoh, M. *Jpn. J. Appl. Phys.* **1996**, *35*, L126.
(16) Li, A. P.; Müller, F.; Birner, A.; Nielsch, K.; Gösele, U. *J. Appl. Phys.* **1998**, *84*, 6023.
(17) Jung, M.; Mho, S. I.; Park, H. L. *Appl. Phys. Lett.* **2006**, *88*, 133121.
(18) Masuda, H.; Nagae, M.; Morikawa, T.; Nishio, K. *Jpn. J. Appl. Phys. 2* **2006**, *45*, L406.
(19) Jessensky, O.; Müller, F.; Gösele, U. *Appl. Phys. Lett.* **1998**, *72*, 1173.
(20) Parkhutik, V. P.; Shershulsky, V. I. *J. Phys. D: Appl. Phys.* **1992**, *25*, 1258.
(21) Skeldon, P.; Thompson, G. E.; Garcia-Vergara, S. J.; Iglesias-Rubianes, L.; Blanco-Pinzon, C. E. *Electrochem. Solid-State Lett.* **2006**, *9*, B47.
(22) Garcia-Vergara, S. J.; Skeldon, P.; Thompson, G. E.; Habazaki, H. *Electrochim. Acta* **2006**, *52*, 681.
(23) Crossland, A. C.; Habazaki, H.; Shimizu, K.; Skeldon, P.; Thompson, G. E.; Wood, G. C.; Zhou, X.; Smith, C. J. E. *Corros. Sci.* **1999**, *41*, 1945.
(24) Skeldon, P.; Thompson, G. E.; Wood, G. C.; Zhou, X. *Philos. Mag. A* **1997**, *76*, 729.
(25) Lee, W.; Schwirn, K.; Steinhart, M.; Pippel, E.; Scholz, R.; Gösele, U. *Nat. Nanotechnol.* **2008**, *3*, 234.
(26) Zhu, X. F.; Li, D. D.; Song, Y.; Xiao, Y. H. *Mater. Lett.* **2005**, *59*, 3160.
(27) Thompson, G. E.; Furneaux, R. C.; Wood, G. C.; Richardson, J. A.; Goode, J. S. *Nature* **1978**, *272*, 433.
(28) Thompson, G. E.; Wood, G. C. *Nature* **1981**, *290*, 230.

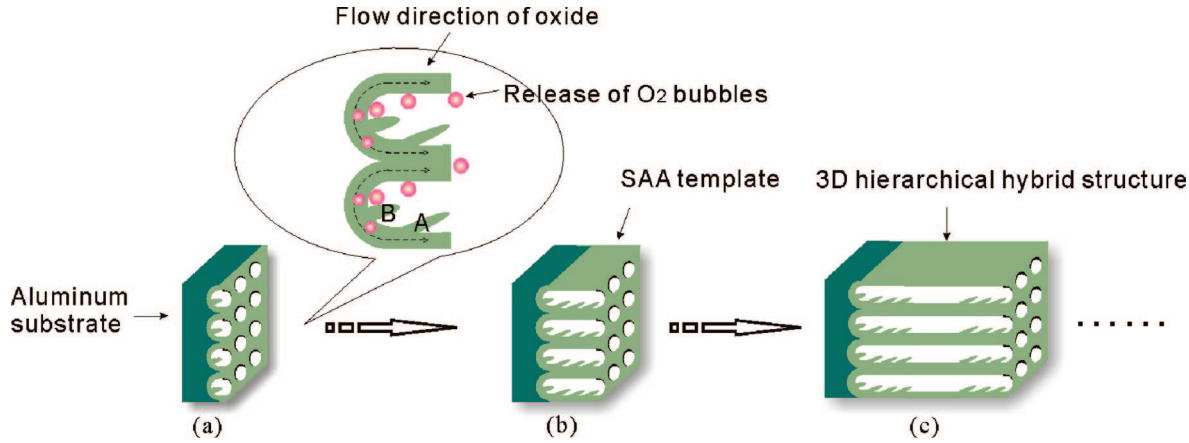

Figure 2. Schematic diagram of SAA synthesis. (a) One serrated branch is generated at the initial stage. Inset: illustration of the evolution of serrated channels. The as-formed serration (branch "A") is pushed upward from the pore bottom to the membrane boundary followed by generating new branch (branch "B"). (b) Serrated branch arrays are formed in the AAO channels. (c) Mutilayer serrated/straight structures are constructed by a successive anodization process in phosphoric and oxalic acid solution.

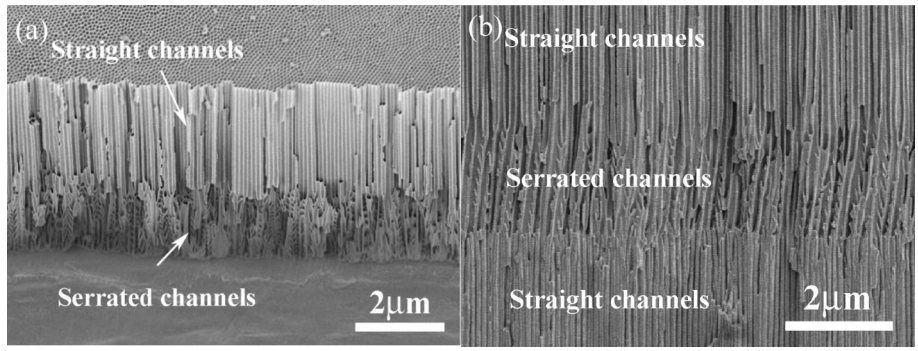

Figure 3. SEM images of AAO template with (a) bilayer (straight + serrated) and (b) trilayer (straight + serrated + straight) structures.

in Figure 2), and the serrated channels are only found on the lower side of the stem pore. This manifests that the serrated channels are molded from the release of the O_2 gas at the pore bottom, and the bubble release direction occurs at an oblique angle. Under compressive stress from continued anodization and generation of O_2 bubbles, the as-formed branches (e.g., branch "A" as labeled in Figure 2 inset) will be pushed toward the membrane boundary followed by generation of new branches (e.g., "B"). Considering that the membrane growth rate is about 4 μm/h and the interval distance of serrated channels ~250 nm, the rate of generating one serrated branch (i.e., discharge one O_2 gas bubble) at the pore base is ~4 min. And because of the vertical placement of Al foil in the electrochemical cell, the upward release direction of the gas bubbles and the flow of oxide materials result in serrated branches aligned mainly on one side.

To construct a 3D hierarchical hybrid structure, aluminum was anodized under 45 V alternately in oxalic acid (5 °C) and phosphoric acid (22 °C) to form layers of straight and serrated channels (as illustrated in Figure 2c). The distinct interface between the serrated and straight channels is displayed in Figure 3a. Higher order layered structures have been created as shown in Figure 3b. Switching the electrolyte from phosphoric acid to oxalic acid results in a new layer consisting of purely straight channels. The achievement of such multilayer architecture further verifies the formation mechanism, that is, the generation of the serrated branch is due to oxygen bubble molding, which initiates at the pore bottom and not on the channel walls.

The novel structures serve as a flexible template to design and synthesize nanowires with sawtooth arrays or straight/sawtooth hybrid structures. In this paper, we present platinum serrated nanowires electrodeposited in the template to reveal the inside structure. Pt-based nanostructures have been widely used as catalysts in the area of fuel cell,[29,30] oil cracking,[31] and electrochemical sensors.[32] The particle size and crystallographic orientation play an important role in their electrocatalytic activities.[8,33,34] Using alternating voltage electrodeposition, high density Pt nanowire arrays are obtained with both straight and serrated channels.

Figure 4a depicts the free-standing Pt serrated nanowires (SENWs) obtained after removal of the template in 1 M NaOH solution. An individual nanowire laid on the Si/SiO_2 surface is shown in Figure 4b. The interval distances (D_b), branch length (l_b), and total wire length are about 250 nm,

(29) Casado-Rivera, E.; Volpe, D. J.; Alden, L.; Lind, C.; Downie, C.; Vazquez-Alvarez, T.; Angelo, A. C. D.; DiSalvo, F. J.; Abruna, H. D. *J. Am. Chem. Soc.* **2004**, *126*, 4043.
(30) Liu, F.; Lee, J. Y.; Zhou, W. J. *J. Phys. Chem. B* **2004**, *108*, 17959.
(31) Domine, M. E.; Iojoiu, E. E.; Davidian, T.; Guilhaume, N.; Mirodatos, C. *Catal. Today* **2008**, *565*, 133–135.
(32) Baranov, A.; Fanchenko, S.; Calliari, L.; Speranza, G.; Minati, L.; Kharitonov, S.; Fedoseenkov, D.; Shorokhov, A.; Nefedov, A. *Surf. Interface Anal.* **2006**, *38*, 823.
(33) Subhramannia, M.; Ramalyan, K.; Pillal, V. K. *Langmuir* **2008**, *24*, 3576.
(34) Yahikozawa, K.; Fujii, Y.; Matsuda, Y.; Nishimura, K.; Takasu, Y. *Electrochim. Acta* **1991**, *36*, 973.

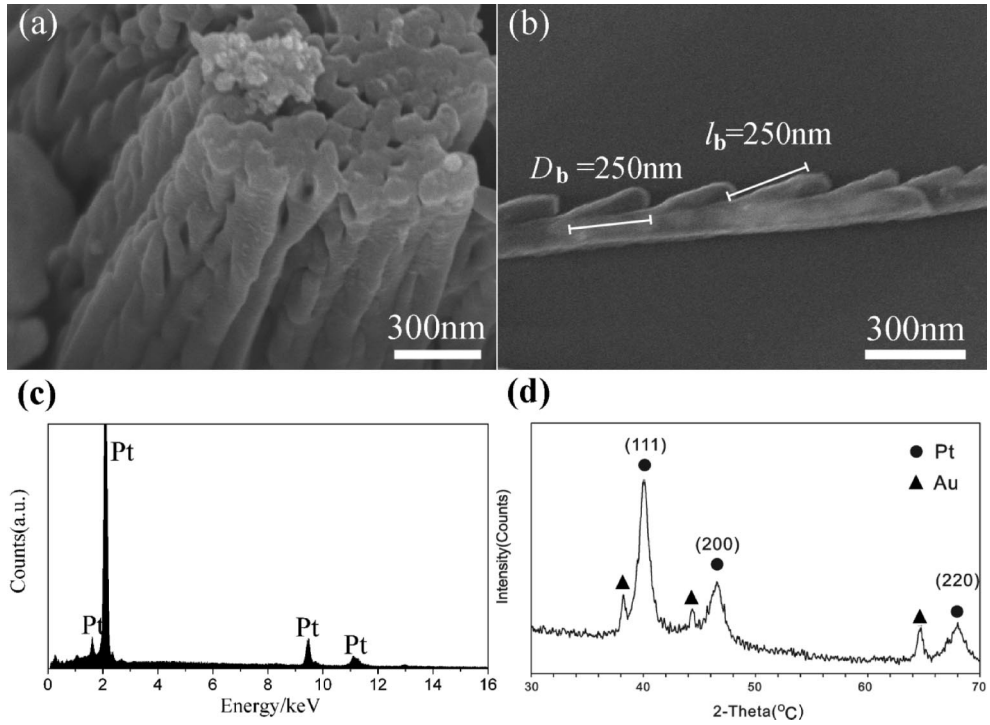

Figure 4. SEM images of (a) free-standing Pt nanowire arrays and (b) an individual nanowire laid on the Si/SiO_2 surface with sawtooth branches. (c) An EDX spectrum of a SENW array. (d) An XRD pattern of SENWs embedded in AAO template indicate the crystal planes of the Pt fcc phase.

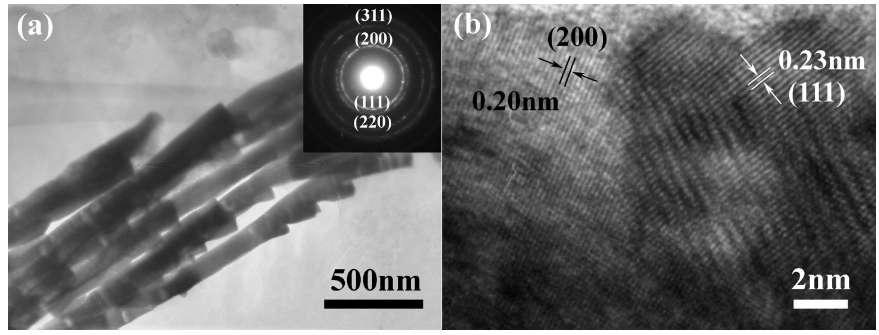

Figure 5. (a) TEM image of serrated Pt nanowires. Inset: corresponding polycrystalline electron diffraction pattern. (b) A high-resolution TEM image of Pt nannowire. The lattice fringes of Pt (111) and (200) planes are labeled with the interplane distances of 0.23 and 0.20 nm, respectively.

250 nm, and 4 μm, which are in accordance with the serrated channel spacing (D_c), length (l_c), and template thickness. Figure 4c is an energy dispersive X-ray analysis (EDX) spectrum of the sample shown in Figure 4a, which confirms that the obtained nanowires consist of pure platinum.

From the X-ray diffraction (XRD) pattern presented in Figure 4d, three peaks are found at 39.8°, 46.2°, and 67.5° which are indexed respectively to the (111), (200), and (220) planes of face-centered cubic (fcc) platinum phase (PDF no. 04-0802). The other peaks are attributed to the fcc Au back electrode (PDF no. 04-0784). The (111) XRD peak is selected to estimate the average grain size (d) of the polycrystalline Pt nanowires based on Scherrer's equation ($d = 0.89\lambda/(\beta \cos \theta)$, where $\lambda = 1.5418$ Å (Cu Kα) and β is the full width at half-maximum of the peak at the diffraction angle θ), yielding $d \approx 6.2$ nm.

Figure 5a displays a transmission electron microscope (TEM) image of a bundle of SENWs. The serrated branch arrays are clearly seen from the image, consistent with the SEM results in Figure 4b. The inset of Figure 5a depicts a selected area electron diffraction (SAED) pattern, verifying that the Pt nanowires have fcc polycrystalline structure. Figure 5b represents a high resolution TEM image of Pt nanowire where (111) and (200) crystalline planes are observed. The crystal sizes are found to be in the range of 5−9 nm, which are in close agreement with the XRD result.

Shape is as important as size in tailoring functionalized nanostructures. As a result of the unique structure of serrated Pt nanowire, it is expected that they exhibit superior electrocatalytic properties as compared to traditional straight wires. Thus, to evaluate this, the electrocatalytic activities of serrated and straight nanowires of the same length are characterized for methanol oxidation. Figure 6a plots the cyclic voltammograms (CV) of methanol electro-oxidation for straight and serrated Pt nanowire arrays in N_2 saturated 2 M CH_3OH + 0.1 M H_2SO_4 solution at 22 °C. The CV curves are measured at a scan rate of 50 mV/s. It is widely accepted that the electro-oxidation consists of several steps and generates strongly adsorbed intermediates on the plati-

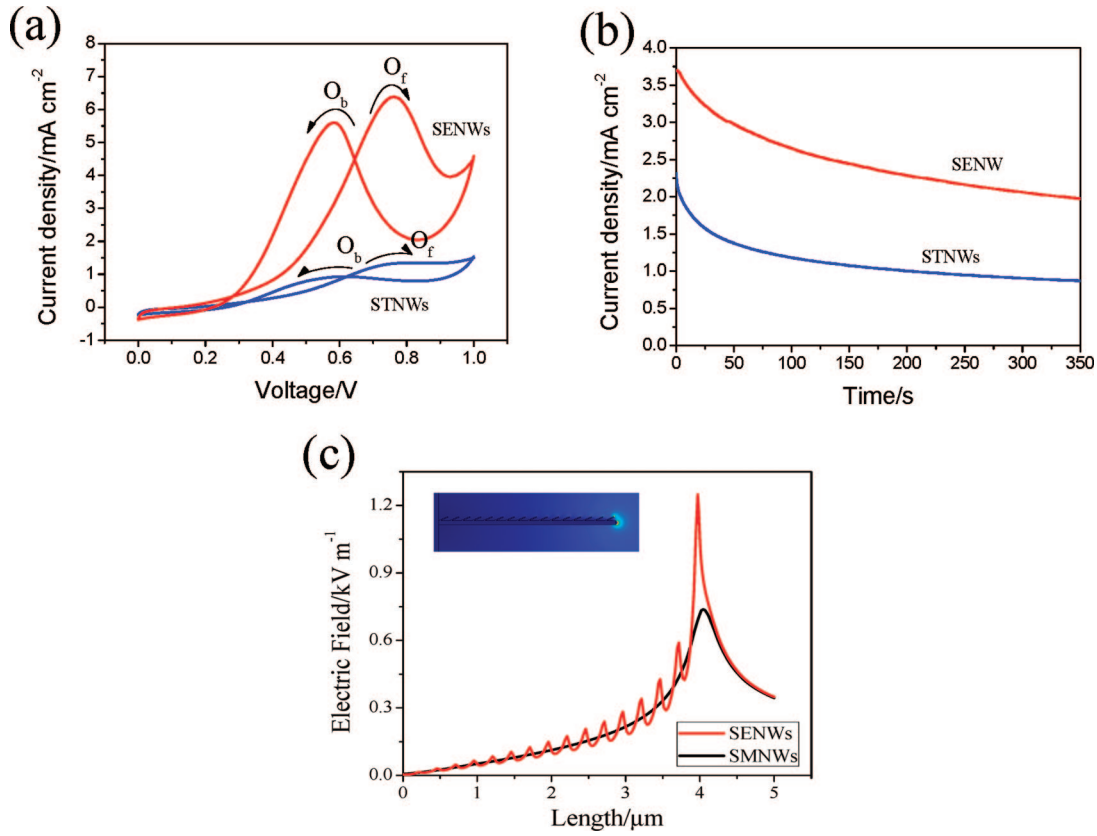

Figure 6. (a) Cyclic voltammograms on serrated (red) and straight (blue) Pt nanowire arrays show a negative shift of the anodic peak by ~70 mV with increased magnitude. (b) Corresponding chronoamperometric curves of the Pt nanowire arrays indicate more active sites remain on SENWs as compared to STNWs. (c) Electric field simulation by COMOSL demonstrates the enhanced field strength around serrated tips. Inset: electric potential map of a serrated nanowire.

num surface in the forward scan ($CH_3OH + 6Pt \rightarrow Pt_2CO + 4Pt + 4H^+ + 4e^-$).[35] And part of the products react with adsorbed OH_{ad} group to form CO_2 and H_2O via the reaction $Pt_2CO + 2OH_{ad} \rightarrow 2Pt + CO_2\uparrow + H_2O$. The unreacted Pt-bridging CO_{ad} can rearrange itself to form a linearly bound carbonaceous species (Pt═C═O), which acts as a poisoning site to inhibit catalytic reaction. In the forward scan of the CV curve (shown in Figure 5a), an anodic peak O_f (j_f = 1.35 mA/cm^2) is observed for straight nanowires (STNWs) at a peak voltage V_f = 0.83 V. In comparison, for the SENWs, the peak is shifted negatively by about 70 mV and the magnitude of j_f increases to 6.38 mA/cm^2, demonstrating a much enhanced electrocatalytic activity. The reverse anodic peak (O_b) is believed to originate from the removal of the linearly bounded carbonaceous species, suppressing the reduction peak at the same potential.[35] For the SENWs electrode, the O_b peak also exhibits a larger current density around 5.6 mA/cm^2.

The comparison of chronoamperograms measured at 0.66 V and 22 °C is shown in Figure 6b. The current density for SENWs is notably higher than that of STNWs. In addition, it decreases to 53.6% of the initial value in 350 s, whereas the current density of STNWs reduces to 37.6% of the initial value after the same duration. Given that the length and filling rate of both nanowires are similar, the more gradual decay of the current densities in serrated nanowires indicates less accumulation of poisoning carbonaceous species on the Pt surface; that is, more active sites remain on SENWs (~53.6%) as compared to STNWs (~37.6%). To investigate the enhanced electrocatytic activities, the electric field distribution is simulated by COMOSL Multiphysics on a single nanowire. The configurations of both SENW and STNW are set according to the SEM results, while the potential between working and counter electrode is set as 1 V. From electric field strength simulation (as plotted in Figure 6c), the amplitude of the electric field is shown to be much enhanced at the serrated tips as compared to straight nanowire. Therefore, in addition to the increased surface area per unit Pt mass, we believe that the strengthened electric field around the serrated tips contributes predominantly to the enhanced electrocatalytic activities.

4. Conclusions

In summary, we have presented a simple and innovative method to fabricate self-assembled AAO templates with periodic serrated structures. The three-dimensional structures with straight and serrated nanochannels are subsequently fabricated by applying anodization in oxalic and phosphoric acid successively. The robust and versatile method can be broadly used to fabricate metallic, semiconductor, and polymer nanowires and nanotubes with flexibly controlled serrated branches. As a demonstration, this paper shows that the serrated Pt nanowires exhibit a high performance of electrocatalytic activities as compared to the straight nanowires. The novel nanostructures promote strong interests in fluid transport, designing and fabricating hierarchical serrated/straight hybrid nanostructures, and are expected to

render various applications in the areas of sensors, catalysts, gene delivery, and biomolecular separations.

Acknowledgment. The authors thank Prof. Gerd Bergmann, Prof. Xufei Zhu, and Dr. Ye Song for their helpful discussions, Dr. Guozheng Shen for TEM imaging, and Mr. Zuwei Liu for technical assistance. The work is supported by NSF Grant DMR 0742225. D.L. is also grateful for the support of the China Scholarship Council and the International Scientific Collaboration Fund of Shanghai (08520705300).

CM8022242

(35) Manoharan, R.; Goodenough, J. B. *J. Mater. Chem.* **1992**, *2*, 875.